
Article:
Entwistle, T. orcid.org/0000-0002-4980-1365, Sanchez-Perez, E., Murray, G.J. et al. (2 more authors) (2022) Co-precipitation synthesis of nickel-rich cathodes for Li-ion batteries. Energy Reports, 8 (Supplement 11). pp. 67-73. ISSN 2352-4847

https://doi.org/10.1016/j.egyr.2022.06.110

Available online at www.sciencedirect.com
ScienceDirect
Energy Reports 8 (2022) 67–73
www.elsevier.com/locate/egyr

Multi-CDT Conference on Clean Energy and Sustainable Infrastructure, Professor Solomon Brown, 5th and 6th April 2022, The University of Sheffield

Co-precipitation synthesis of nickel-rich cathodes for Li-ion batteries

Thomas Entwistle[a,*], Enrique Sanchez-Perez[b], Glen J. Murray[b], Nirmalesh Anthonisamy[b], Serena A. Cussen[b]

[a] *Department of Chemical and Biological Engineering, Sir Robert Hadfield Building, Mappin St, University of Sheffield, Sheffield, S1 3JD, UK*
[b] *Department of Materials Science and Engineering, Sir Robert Hadfield Building, Mappin St, University of Sheffield, Sheffield, S1 3JD, UK*

Received 14 June 2022; accepted 25 June 2022
Available online 13 July 2022

Abstract

The preparation of Ni-rich cathode materials is challenging due to the Ni^{2+} ion sensitivity to oxidation during synthesis. The synthesis conditions during the manufacture of Ni-rich materials such as $LiNi_{0.8}Mn_{0.1}Co_{0.1}O_2$ (NMC811) therefore require stringent control. The co-precipitation step, applied in the synthesis of the metal hydroxide precursor, determines the secondary particle assembly formation, where it is typically desirable to produce uniform, spherical, ∼10 μm-diameter structures. A stirred tank reactor is often employed to maintain a constant temperature of 60 °C and a controlled pH of between 10.5 and 11.5 in an inert atmosphere to maintain a high Ni^{2+}/Ni^{3+} ion ratio. This promotes the formation of an NMC hydroxide precursor ($Ni_xMn_yCo_z(OH)_2$) which is typically milled with a lithium salt and calcined to form $LiNi_xMn_yCo_zO_2$ with a layered α-$NaFeO_2$ crystalline structure. This review outlines some of the critical synthetic parameters for the formation of spherical secondary assemblies of metal hydroxide precursors for nickel-rich layered cathodes.

Peer-review under responsibility of the scientific committee of the Multi-CDT Conference on Clean Energy and Sustainable Infrastructure, Professor Solomon Brown, 2022.

Keywords: Lithium-ion; Batteries; NMC; Synthesis; Co-precipitation

1. Introduction

Cathode materials remain a focal point of battery research due to the high proportion of raw material costs associated with their production and their capacity limitation in comparison to graphite anodes [1,2]. The development of lithium-ion batteries towards an electric vehicle range of 300 miles relies on cathode materials with energy densities of 760 Wh kg^{-1} (or 200 mAh g^{-1}) [3–5]. Lithium-ion batteries initial success came *via* the commercialisation of $LiCoO_2$ (LCO) which can deliver a practical capacity of 130 mAh g^{-1} (less than half of its 274 mAh g^{-1} theoretical capacity). [5] This is a result of the structural stability of Li_xCoO_2 declining when $x < 0.5$ [6,7]. Ethical, economic and environmental concerns continue to encourage the minimisation of cobalt in cathode materials [5–9].

* Corresponding author.
E-mail addresses: tentwistle1@sheffield.ac.uk (T. Entwistle), s.cussen@sheffield.ac.uk (S.A. Cussen).

https://doi.org/10.1016/j.egyr.2022.06.110

Peer-review under responsibility of the scientific committee of the Multi-CDT Conference on Clean Energy and Sustainable Infrastructure, Professor Solomon Brown, 2022.

Developments to improve the cathode capacity have also focused on the partial replacement of cobalt with other transition metals such as nickel, manganese and aluminium. One alternative, lithium nickel oxide ($Li_{1-x}Ni_xO_2$, LNO), has a similar theoretical capacity of 275 mAh g^{-1} but displays much higher reversible capacities of 200–220 mAh g^{-1} [5]. One major challenge with LNO is the reduction of Li:Ni stoichiometry during synthesis, where lithium deficiencies can result as well as poor electrochemical capacity retention due to secondary particle failure; this is caused by a crystalline volume change during the H2-H3 phase transition [5,10,11].

To utilise the high capacity offered by LNO while mitigating these stability issues, manganese, cobalt and aluminium have been used as stabilising agents to form nickel–manganese–cobalt oxide and nickel–cobalt–aluminium oxide (commonly abbreviated to NMC and NCA respectively). Cobalt provides structural stability and mitigates Li/Ni cation mixing [12] while aluminium and manganese can provide thermal and further structural stability during cycling [5,12,13]. NMC111 (where the nickel: manganese: cobalt ratio is 1:1:1) can deliver capacities of ∼160 mAh g^{-1} (cycled at 2.7–4.2 V) compared to a theoretical capacity of 277.8 mAh g^{-1} and high capacity retention of 92.4% over 100 cycles (cycled at 3.0–4.3 V, 25 °C) [4,14]. Moving closer to a target of 200 mAh g^{-1} requires an increase in nickel content, with stoichiometries such as NMC532, NMC622 and NMC811.

Progressing to nickel content above 80% leads to increases in capacity, but more pronounced thermal and cycling instabilities, as seen in Fig. 1 [4]. The increased presence of reactive Ni^{4+} ions in the delithiated state initiates an aggressive reaction with the electrolyte, consuming active material and forming a surface rock-salt layer [14–16]. For the NMC variants, nickel contents of up to 95% have been reported, with 88% nickel content for NCA materials [13,17].

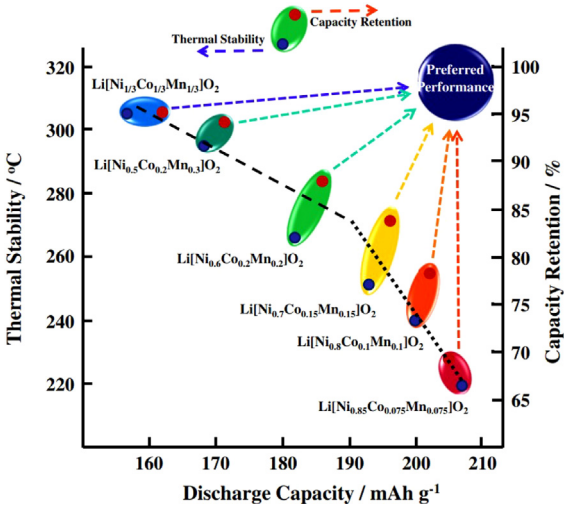

Fig. 1. The change in specific capacity and capacity retention as the transition metal ratio changes in NMC cathode materials. The capacity retention relates to the capacity retained after 100 cycles at 0.5 C [4].

Transition metal oxide cathode materials may be synthesised by a variety of routes, including solid-state, high temperature [18,19]; hydrothermal [20]; and co-precipitation methods [13,21–23]. The co-precipitation synthesis route involves mixing stoichiometric transition metal salts with a basic precipitating agent and a complexing agent to produce a mixed-transition metal ion precursor to the final lithiated oxide product [13,21]. Co-precipitation affords control over multiple reaction conditions, allowing the morphology and tap density to be tailored. This is typically achieved by tuning the pH, stirring rate, temperature, and reaction time to form quasi-spherical particles; these parameters change depending on the transition metal ratio of the material [21,24].

The NMC precursor subsequently undergoes lithiation and calcination steps to afford the final '$LiNi_xMn_yCo_zO_2$' layered NMC oxide with an α-$NaFeO_2$ crystal structure. This structure consists of stacked layers of lithium, and transition metal oxide, with 2-dimensional channels for the lithium ions to (de)intercalate easier in/out of the structure during cycling [25]. The lithiation of the dried precursor involves homogeneous mixing with stoichiometric

amounts of a lithium source. Typically, an excess of lithium source is used (Li:*M* ratio of 1.01–1.05:1) [15,26–28]. Calcination temperatures of between 700–800 °C are commonly applied for NMC materials with Ni > 80%, but this calcination temperature is typically optimised for nickel content [4,24,29,30]. An oxidising atmosphere is recommended for the calcination of layered $LiNi_xMn_yCo_zO_2$ to prevent cation mixing of Ni^{2+} ions to Li sites due to the similar ionic radii of Ni^{2+} and Li^+ (0.69 Å vs 0.76 Å) [31,32]. Two recent reviews by Kurzhals and Riewald et al. elegantly details the effects of calcination conditions on resulting structural chemistry and primary particle morphology [33,34].

Here, we review published findings on the co-precipitation synthesis of the metal hydroxide precursor in an attempt to draw together the effects of key parameters such as pH, temperature, reaction time and reactant concentrations on resulting secondary particle formation.

2. Precursor synthesis

The precursor synthesis stage involves a reaction between stoichiometric quantities of transition-metal salts nickel, manganese, and cobalt hydrated sulphates ($NiSO_4.6H_2O$, $MnSO_4.H_2O$ and $CoSO_4.7H_2O$ respectively); using ammonia as a complexing agent, and a base [4,15]. Ammonia is often added first to provide a sufficient concentration gradient to promote the formation of $[M(NH_3)]^{2+}$ complexes prior to particle precipitation [21]. Sodium hydroxide is typically chosen as the base to maintain a high pH and supply hydroxide ions for NMC precursor precipitation while maintaining lower costs per high purity than other hydroxide bases such as potassium hydroxide. For nickel-rich materials, $LiOH.H_2O$ is usually selected as the lithium source due to its lower thermal decomposition temperature range of 230–380 °C [35]. This allows the calcination temperature to be kept at a suitably low temperature to minimise oxygen loss from the layered cathode compound and the resultant formation of the undesired rock-salt phase [5,35,36]. Li_2CO_3 can be used for lower nickel-content material such as NMC532 or NMC111, but due to its increased thermal decomposition temperature of 725 °C [5,35], it is not frequently used for more nickel-rich materials [1,37].

Co-precipitation reaction mechanisms are complex and rely on the control of multiple parameters, with the added difficulty of each Ni, Mn and Co ion ratio requiring different conditions to ensure uniform precipitation in each NMC system. For example, one may apply lower pH conditions for a higher Mn/Co content, with pH values of 9.8–10 producing optimal tap density of 1.0 g cm^{-3} for $Ni_{0.33}Mn_{0.33}Co_{0.33}(OH)_2$ ($NMC111(OH)_2$) particles, whereas pH values of 10.8–11.4 are applied for the synthesis of $Ni(OH)_2$ with an increased tap density of 1.5–1.7 g cm^{-3} [21,24]. These conditions should be maintained for the complexing and precipitation of the metal ions to occur in such a manner so as to promote the formation of a layered transition metal hydroxide as shown in general scheme 1 and 2 respectively. These schemes provide an overview of the reaction, where *n* represents the number of coordinating ammonia molecules, which is less than or equal to 6 [21,38]. The β-NMC hydroxide material obtained by this co-precipitation reaction crystallizes in a brucite type structure, with a hexagonal $P\bar{3}m1$ space group [39]. Care must be taken as the divalent metal ions can oxidise to their trivalent states, which can lead to undesirable side-phases or disruptions to the layered structure which can have a deleterious effect during calcination [38,40,41]. Additionally, reaction temperatures are also limited to 60 °C as higher residence temperatures can lead to increases in primary particle size and tap density [21,24].

$$M^{2+} + n\mathrm{NH_3} \rightarrow \left[M\,(\mathrm{NH_3})_n\right]^{2+} \qquad \text{Scheme 1 [21]}$$

$$\left[M\,(\mathrm{NH_3})_n\right]^{2+} + 2\mathrm{OH^-} \rightarrow M\,(\mathrm{OH})_2 + n\,(\mathrm{NH})_3 \qquad \text{Scheme 2 [21]}$$

The concentration of the transition metal solution, ammonia, and sodium hydroxide also affect the particle size and tap density. Typically, the total transition metal sulphate concentration is 2 M [4,41]. Wang et al. synthesized NMC-80:05:15-$(OH)_2$ with a variety of NH_3: NaOH molar ratios, concluding that a ratio of 1:1 yields an optimised particle size, tap density and uniformity, with nanoplate primary particles of >100 nm and ∼20 μm spherical secondary particles with a density of 1.5 g cm^{-3}. Other ratios produced clustered, irregular particles of less than 10 μm in diameter and with tap densities of less than 0.8 g cm^{-3} [41].

The ammonia: transition metal ratio also affects $NMC811(OH)_2$ particle morphology and tap density due to its ability to complex with transition metal ions prior to particle precipitation. Increasing the NH_3:*M* ratio from 1.0–1.2:1 leads to smaller primary particle grains, less uniformity in secondary particle morphologies and a narrower particle size distribution [24,42]. A ratio of 1:1 was found to yield spherical, uniform particles of ∼20 μm with a density of 2.0 g cm^{-3} [43]. An increased ammonia: transition metal ratio of 1.2:1 can also yield quasi-spherical

particles with a 10 μm diameter for nickel contents of between 60% and 95% [15], but the concentration of $[Ni(NH_3)_6]$ complexes can increase, decreasing the precipitation rate of nickel [24]. Higher concentrations of ammonia can be detrimental to the particle morphology, leading to the formation of 'clusters' with non-uniform particle sizes and shapes, with each secondary particle ranging from 5–15 μm [43]. This is associated with the incomplete precipitation of $NMC811(OH)_2$ and the formation of $[Ni(NH_3)_n]^{2+}$ complex [24].

The pH of the system is determined by the ammonia: sodium hydroxide solution and can dictate the degree of transition metal precipitation. Its addition is often controlled *via* a pH meter. The pH-variable solubility of each transition metal complex $[M(NH_3)_n]^{2+}$ means there is an optimum pH value which varies depending on the NMC ratio. For instance, van Bommel et al. showed that synthesizing a $Ni_{0.33}Mn_{0.33}Co_{0.33}(OH)_2$ precursor at pH ∼9.8 produces a peak tap density of 1.0 g cm^{-3}, whereas $Ni(OH)_2$ synthesized at 10.2–11.5 has an increased tap density of 1.5 g cm^{-3} [21]. This is supported by Liang et al. who reported that $NMC622(OH)_2$ synthesized *via* co-precipitation had a more spherical morphology at pH 11.2 and an increased tap density of 1.65 g cm^{-3}, compared with pH values of 11.5 and 11.8, which had a tap densities of 1.47 and 1.05 g cm^{-3} respectively as well as a less uniform morphology displayed in Fig. 2 [44]. Furthermore, Vu et al. demonstrated that $NMC811(OH)_2$ particles were near-uniform in size and had an increased tap density of 1.91 g cm^{-3} when synthesized at pH 11.5 compared to pH 11.8 (which yields a tap density of 1.26 g cm^{-3}) [24]. For lower nickel-content cathode materials ($NMC111(OH)_2$), a pH of 11.0 is reported to be optimal with respect to morphology, with a decreasing particle size (10 μm to ∼3 μm), tap density (1.79 to 1.11 g cm^{-3}) and uniformity as pH increases from 11.0 to 12.0 [42]. A similarly low tap density of 1.0 g cm^{-3} achieved by synthesizing $NMC111(OH)_2$ at pH 10 [21]. Below these optimal pH values, there are excess nickel and manganese ions in the system, leading to the formation of unwanted side products [45]. Accordingly, one experiment demonstrated that a pH of 10.6 in the synthesis of $NMC111(OH)_2$ was found to yield larger (median size of 16 μm), more uniform particles with an increased tap density (1.23 g cm^{-3}) and higher capacity retention after 50 cycles (96.5%) than equivalent materials prepared at a pH of 11.4 (which had a median size of 8 μm, a tap density of 0.3 g cm^{-3}, and a capacity retention of 93.6%) [46].

The vessels employed in the co-precipitation reactions are round-bottom flask reactors or stirred tank reactors (STRs) and are typically operated in batch mode. While round bottom flask reactors have a simpler setup, this comes at a cost to experimental control (specifically the difficulties with *operando* monitoring of multiple parameters), limitations over the geometry of the vessel, absence of an agitator (which is often substituted for a magnetic stirrer bar) and limitations over scale-up potential. In contrast, STRs enhance the synthesis control through a real-time feedback response to parameters such as pH and temperature and have an agitator and baffles that promote homogeneous distribution and mixing of contents. STR vessels also have the capability to scale up through geometric resizing of the vessel or the conduction of the reaction in a continuous manner by continually pumping reactants in and extracting the wetted precipitated product [47,48].

In terms of mixing, the type of impeller blade impacts the nature and direction of the mixing (radial, axial or both) and determines the distribution of particles and homogeneity of the system. Another important factor is the stirring rate, which controls the shear rate of the system and consequently can affect the particle growth [47]. The type of the impeller blade can impact the tap density and particle size of the cathode precursors due to the direction of the fluid flow through the blade. Zhu et al. [49] investigated the effect of axial mixing propeller turbines compared to radial flow impellers and axial and radial flow impellers. The propeller turbine used at 1100 rpm led to $NMC622(OH)_2$ precursor particles with an increased tap density of 2.0 g cm^{-3} which increased to 2.5 g cm^{-3} upon calcination, with no change in average particle size (∼12 μm) on sintering. The initial discharge capacity of the resultant NMC622 cells was 177.6 mAh g^{-1} (2.7–4.3 V, 0.2C), with 97.9% capacity retention after 200 cycles at 2C, with comparative impeller blades such as the flat-blade and Rushton turbines displaying a 10–15% reduction in capacity and capacity retention [49]. A stirring rate can also influence the secondary particle size. Commonly, a stirring rate of 1000 rpm is used for NMC synthesis, yielding a particle size of 8–12 μm and tap densities on the order of 2.0 g cm^{-3} (though these properties also depend on other reaction conditions) [21,50,51]. Vu et al. found that a lower stirring rate (500 rpm) produced larger mean particle sizes (20 μm), compared to 800 rpm (13 μm) [24].

There are other established factors that affect the mixing characteristics and consequently the particle characteristics, such as reactor geometry and its configuration (i.e. the inclusion of baffles, liquid level and turbine depth). This raises an interesting prospect when considering the scale up of this reaction [48]. Longer reaction times generally lead to more spherical particle morphologies and a higher tap density [21,49]. Due to the differing vessels, agitators, and resultant shear rates of the system, optimal residence times vary across systems. For this reason, residence

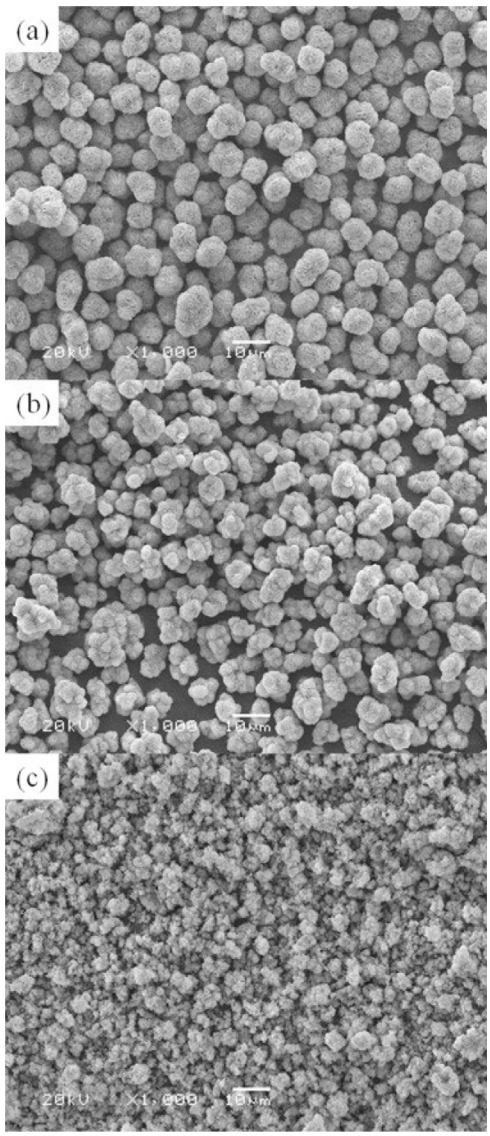

Fig. 2. Scanning electron microscope images of $Ni_{0.6}Mn_{0.2}Co_{0.2}(OH)_2$ synthesized via a co-precipitation technique at various pH. (a) pH of 11.2; (b) pH of 11.5; (c) pH of 11.8 [44].

times vary in the literature spanning between 4 and 27 h for co-precipitation reactions [22,26]. As the 27 h mark is approached, the particle size tends to plateau as particles begin to mature rather than grow, allowing the possibility for a continuous flow system to be developed to yield consistently-sized particles [43].

3. Conclusion

High nickel-content cathode precursors synthesised *via* the co-precipitation route require careful control over several key reaction parameters to produce particles with desired size, shape and tap density. The formation of Ni-rich cathode materials is favoured by milder temperatures of ∼60 °C and anaerobic conditions to prevent the oxidation of Ni^{2+}.

The precipitation of the transition metals to form the preferred quasi-spherical ∼10 μm diameter secondary particles requires a basic precipitating agent and a complexing agent. Sodium hydroxide is typically used to control

the pH of the solution, with a pH range of between 11.0 and 11.5 favoured for NMC811$(OH)_2$ precursor synthesis. The molar ratio of transition metal: ammonia complexing agent should also be optimised for the resulting chemistry to acquire optimised secondary assembly size and tap densities of $\sim$2.0 g cm^{-3} for the NMC hydroxide precursor.

Declaration of competing interest

The authors declare that they have no known competing financial interests or personal relationships that could have appeared to influence the work reported in this paper.

Acknowledgements

TE and SC thank the EPSRC, UK for financial support via grant EP/L016818/1 which funds the Centre for Doctoral Training in Energy Storage and its Applications. ES-P, GM, NA and SC gratefully acknowledge the support of the Faraday ISCF Faraday Challenge projects FutureCat, UK [grant no. FIRG017] and Degradation, UK [grant no. FIRG001] and the EPSRC, UK [EP/W018950/1].

References

[1] Ahmed S, Nelson PA, Gallagher KG, Susarla N, Dennis DW. Cost and energy demand of producing nickel manganese cobalt cathode material for lithium ion batteries. J Power Sources 2017;342:733–40.
[2] Reuter F, Baasner A, Pampel J, Piwko M, Dörfler S, Althues H, et al. Importance of capacity balancing on the electrochemical performance of $Li[Ni_{0.8}Co_{0.1}Mn_{0.1}]O_2$ (NCM811)/Silicon full cells. J Electrochem Soc 2019;166:A3265.
[3] Giffi C, Vitale Jr. J, Drew M, Kuboshima Y, Sase M. Unplugged: Electric vehicle realities versus consumer expectations. United States: Deloitte Global Services Limited; 2011.
[4] Noh H-J, Youn S, Yoon CS, Sun Y-K. Comparison of the structural and electrochemical properties of layered $Li[Ni_xCo_yMn_z]O_2$ (x = 1/3, 0.5, 0.6, 0.7, 0.8 and 0.85) cathode material for lithium-ion batteries. J Power Sources 2013;233:121–30.
[5] Bianchini M, Roca-Ayats M, Hartmann P, Brezesinski T, Janek J. There and back again—The journey of $LiNiO_2$ as a cathode active material. Angew Chem Int Ed 2018;58(31):10434–58.
[6] Whittingham MS. Lithium batteries and cathode materials. Chem Rev 2004;104(10):4271–302.
[7] Radin MD, Hy S, Sina M, Fang C, Liu H, Vinckeviciute J, et al. Narrowing the gap between theoretical and practical capacities in Li-ion layered oxide cathode materials. Adv Energy Mater 2017;7(20):1602888.
[8] Olivetti EA, Ceder G, Gaustad GG, Fu X. Lithium-ion battery supply chain considerations: Analysis of potential bottlenecks in critical metals. Joule 2017;1:229–43.
[9] He L-P, Li K, Zhang Y, Jun L. Structural and electrochemical properties of low-cobalt-content $LiNi_{0.6+x}Co_{0.2-x}Mn_{0.2}O_2$ ($0.0 \leq x \leq 0.1$) cathodes for lithium-ion batteries. Appl Mater Interfaces 2020;12(25):28253–63.
[10] Yoon CS, Jun D-W, Myung S-T, Sun Y-K. Structural stabilty of $LiNiO_2$ cycled above 4.2 V. ACS Energy Lett 2017;2(5):1150–5.
[11] Arai H, Okada S, Ohtsuka H, Ichimura M, Yamaki J. Characterization and cathode performance of $Li_{1-x}Ni_{1+x}O_2$ prepared with the excess lithium method. Solid State Ion 1995;80:261–9.
[12] Li H, Cormier M, Zhang N, Inglis J, Li J, Dahn J. Is cobalt needed in Ni-rich positive electrode materials for lithium ion batteries? J Electrochem Soc 2019;166:A429.
[13] Li W, Lee S, Manthiram A. High-nickel NMA: A cobalt-free alternative to NMC and NCA cathodes for lithium-ion batteries. Adv Mater 2020;2002718.
[14] Jung R, Metzger M, Maglia F, Stinner C, Gastieger HA. Chemical versus electrochemical electrolyte oxidation on NMC111, NMC622, NMC811, LNMO, and conductive carbon. J Phys Chem Lett 2017;8(19):4820–5.
[15] Ryu H-H, Park K-J, Yoon CS, Sun Y-K. Capacity fading of Ni-rich $Li[Ni_xCo_yMn_{1-x-y}]O_2$ ($0.6 \leq x \leq 0.95$) cathodes for high-energy-density lithium-ion batteries: Bulk or surface degradation? Chem Mater 2018;30:1155–63.
[16] White JL, Gittleson FS, Homer M, El Gabaly F. Nickel and cobalt oxidation state evolution at Ni-rich NMC cathode surfaces during treatment. J Phys Chem 2020;124(30):16508–14.
[17] Yoon CS, Ryu H-H, Park G-T, Kim J-H, Kim K-H, Sun Y-K. Extracting maximum capacity from Ni-rich $Li[Ni_{0.95}Co_{0.025}Mn_{0.025}]O_2$ cathodes for high-energy-density lithium-ion batteries. J Mater Chem A 2018;6(9):4126–32.
[18] Mizushima K, Jones P, Wiseman P, Goodenough J. Li_xCoO_2 ($0<x\leq l$): A new cathode material for batteries of high energy density. Mater Res Bull 1980;15:783–9.
[19] Dahn J, von Sacken U, Michal C. Structure and electrochemistry of $Li_{1\pm y}NiO_2$ and a new Li_2NiO_2 phase with the $Ni(OH)_2$ structure. Solid State Ion 1990;44:87–97.
[20] Li Y, Han Q, Ming X, Ren M, Li L, Ye W, et al. Synthesis and characterisation of $LiNi_{0.5}Co_{0.2}Mn_{0.3}O_2$ cathode material prepared by a novel hydrothermal process. Ceram Int 2014;40:14933–8.
[21] van Bommel A, Dahn JR. Analysis of the growth mechanism of coprecipitated spherical and dense nickel, manganese, and cobalt-containing hydroxides in the presence of aqueous ammonia. Chem Mater 2009;21(8):1500–3.
[22] Kim U-H, Jun D-W, Park K-J, Zhang Q, Kaghazchi P, Aurbach D, et al. Pushing the limit of layered transition metal oxide cathodes for high-energy density rechargeable Li ion batteries. Energy Environ Sci 2018;11(5):1271–9.

[23] Zhang N, Li J, Li H, Liu A, Huang Q, Ma L, et al. Structural, electrochemical, and thermal properties of nickel-rich $LiNi_xMn_yCo_zO_2$ materials. Chem Mater 2018;30(24):8852–60.
[24] Vu D-L, Lee J-w. Properties of $LiNi_{0.8}Co_{0.1}Mn_{0.1}O_2$ as a high energy cathode material for lithium-ion batteries. Korean J Chem Eng 2015;33(2):514–26.
[25] Xu J, Lin F, Doeff MM, Tong W. A review of Ni-based layered oxides for rechargeable Li-ion batteries. J Mater Chem A 2017;5(3):874–901.
[26] Lipson AL, Durham JL, LeResche M, Abu-Baker I, Murphy MJ, Fister TT, et al. Improving the thermal stability of NMC 622 Li-ion battery cathodes through doping during coprecipitation. Appl Mater Interfaces 2020;12(16):18512–8.
[27] Zheng J, Yan P, Estevez L, Wang C, Zhang J-G. Effect of calcination temperature on the electrochemical properties of nickel-rich $LiNi_{0.76}Mn_{0.14}Co_{0.1}O_2$ cathodes for lithium-ion batteries. Nano Energy 2018;49:538–48.
[28] Park K-J, Jung H-G, Kuo L-Y, Kaghazchi P, Yoon CS, Sun Y-K. Improved cycling stability of $Li[Ni_{0.90}Co_{0.05}Mn_{0.05}]O_2$ through microstructure modification by boron doping for Li-ion batteries. Adv Energy Mater 2018;8(25):1–9.
[29] Shin H, Kim M, Kim N, Jung C, Chung J, Kim K, et al. Local oxidation states of Ni, Co, and Mn atoms within pristine and charged $Li_xNi_{0.88}Co_{0.08}Mn_{0.04}O_2$ primary particles. J Phys Chem Solids 2021;148:109732.
[30] Yoon CS, Ho Choi M, Lim B-B, Lee E-J, Sun Y-K. Review—High-capacity $Li[Ni_{1-x}Co_{x/2}Mn_{x/2}]O_2$(x = 0.05, 0) cathodes for next-generation Li-ion battery. J Electrochem Soc 2015;162(14):A2483.
[31] Li H, Zhou P, Liu F, Li H, Cheng F, Chen J. Stabilizing nickel-rich layered oxide cathodes by magnesium doping for rechargeable lithium-ion batteries. Chem Sci 2019;10(5):1374–9.
[32] Hua W, Wang K, Knapp M, Schwarz B, Wang S, Liu H, et al. Chemical and structural evolution during the synthesis of layered $Li(Ni, Co, Mn)O_2$ oxides. Chem Mater 2020;32(12):4984–97.
[33] Kurzhals P, Riewald F, Bianchini M, Sommer H, Gasteiger HA, Janek J. The $LiNiO_2$ cathode active material: A comprehensive study of calcination conditions and their correlation with physiochemical properties. Part I. Structural chemistry. J Electrochem Soc 2021;168:110518.
[34] Riewald F, Kurzhals P, Bianchini M, Sommer H, Janek J, Gasteiger HA. The $LiNiO_2$ cathode active material: A comprehensive study of calcination conditions and their correlation with physicochemical properties. Part II. Morphology. J Electrochem Soc 2022;169:020529.
[35] Martinez AC, Grugeon S, Cailleu D, Courty M, Tran-Van P, Delobel B, et al. High reactivity of the nickel-rich $LiNi_{1-x-y}Mn_xCo_yO_2$ layered materials surface towards H_2O/CO_2 atmosphere and $LiPF_6$-based electrolyte. J Power Sources 2020;468:228204.
[36] Dinh L, Mclean II W, Schildbach M, LeMay J, Siekhaus W, Balooch M. The nature and effects of the thermal stability of lithium hydroxide. J Nucl Mater 2003;317(2–3):175–88.
[37] Shunmugasundaram R, Arumugam RS, Dahn J. High capacity Li-rich positive electrode materials with reduced first-cycle irreversible capacity loss. Chem Mater 2015;27(3):757–67.
[38] Hall DS, Lockwood DJ, Bock C, MacDougall BR. Nickel hydroxides and related materials: a review of their structures, synthesis and properties. Proc R Soc Lond Ser A Math Phys Eng Sci 2015;471(2174):20140792.
[39] McEwan RS. Crystallographic studies on nickel hydroxide and the higher nickel oxides. J Phys Chem 1971;75(19):1782–9.
[40] Zhou F, Zhao X, van Bommel A, Rowe AW, Dahn J. Coprecipitation synthesis of $Ni_xMn_{1-x}(OH)_2$ mixed hydroxides. Chem Mater 2010;22(3):1015–21.
[41] Wang D, Belharouak I, Ortega LH, Zhang X, Xu R, Zhou D, et al. Synthesis of high capacity cathodes for lithium-ion batteries by morphology-tailored hydroxide co-precipitation. J Power Sources 2015;274:451–7.
[42] Lee M-H, Kang Y-J, Myung S-T, Sun Y-K. Synthetic optimization of $Li[Ni_{1/3}Co_{1/3}Mn_{1/3}]O_2$ via co-precipitation. Electrochim Acta 2004;50(4):939–48.
[43] Cheralathan K, Kang NY, Park HS, Lee YJ, Choi WC, Ko YS, et al. Preparation of spherical $LiNi_{0.80}Co_{0.15}Mn_{0.05}O_2$ lithium-ion cathode material by continuous co-precipitation. J Power Sources 2010;195(5):1486–94.
[44] Liang L, Du K, Peng Z, Cao Y, Duan J, Jiang J, et al. Co-precipitation synthesis of $Ni_{0.6}Co_{0.2}Mn_{0.2}(OH)_2$ precursor and characterisation of $LiNi_{0.6}Co_{0.2}Mn_{0.2}O_2$ cathode material for secondary lithium ion batteries. Electrochim Acta 2014;130:82–9.
[45] Hy S, Liu H, Zhang M, Qian D, Hwang B-J, Meng YS. Performance and design considerations for lithium excess layered oxide positive electrode materials for lithium ion batteries. Energy Environ Sci 2016;9(6):1931–54.
[46] Feng Z, Barai P, Gim J, Yuan K, Wu YA, Xie Y, et al. In situ monitoring of the growth of nickel, manganese, and cobalt hydroxide precursors during co-precipitaiton synthesis of Li-ion cathode materials. J Electrochem Soc 2018;165(13):A3077–83.
[47] Coulson JM, Richardson JF. Coulson and Richardson's chemical engineering: Volume 1. Oxford: Pergamon Press; 1996.
[48] Green DW, Perry RH. Perry's chemical engineers' handbook. New York: McGraw-Hill Education; 2007.
[49] Zhu Q, Xiao H, Zhang R, Geng S, Huang Q. Effect of impeller type on preparing spherical and dense $Ni_{1-x-y}Co_xMn_y(OH)_2$ precursor via continuous co-precipitation in pilot scale: A case of $Ni_{0.6}Co_{0.2}Mn_{0.2}(OH)_2$. Electrochim Acta 2019;318:1–13.
[50] Xie Q, Li W, Manthiram A. A Mg-doped high-nickel layered oxide cathode enabling safer high-energy-density Li-ion batteries. Chem Mater 2019;31(3):938–49.
[51] Laveda JV, En Low J, Pagani F, Stilp E, Dilger S, Baran V, et al. Stabilizing capacity retention in NMC811/graphite full cells via TMSPi electrolyte additives. Appl Energy Mater 2019;10(2):7036–44.